Article preview

Abstract

Introduction

Section snippets

References (27)

Cited by (10)

Study of NiFeCoCr medium entropy alloy as a binder phase on W–Mo heavy tungsten alloy by secondary ball milling

Chun-Liang Chen [a] ℞ 🖾, Sutrisno [a b]

Show more ⌄

+ Add to Mendeley   ⚬ᶜ Share   🗭 Cite

Get rights and content ↗

Highlights

Study of NiFeCoCr medium entropy alloy as a binder phase on W–Mo heavy tungsten alloy by secondary ball milling

Chun-Liang Chen [a,*], Sutrisna [a,b]

[a] Department of Materials Science & Engineering, National Dong Hwa University, Shou-Feng, Hualien, 97401, Taiwan
[b] Department of Mechanical Engineering, Institut Teknologi Nasional, Yogyakarta, 55281, Indonesia

ARTICLE INFO

ABSTRACT

The binder phase of NiFeCoCr medium entropy alloy (MEA) dispersed in W–Mo heavy tungsten alloy synthesized by secondary ball milling was studied. The results show that the MEA binder phase with a single FCC solid solution structure was obtained after the pre-milling process. A considerable reduction of Cr content in the MEA binder phase encourages the dissolution of Cr into the tungsten matrix and forms the Cr-rich oxides after the sintering process. TEM investigations show that the Cr-rich oxide has been indexed as the $(Cr, Fe)O_3$ and the twinned structure was observed in the FCC MEA binder phase. Besides, as the sintering temperature was increased to 1450 °C, liquid phase sintering is dominant in the model alloys, leading to a decrease in the hardness of the model alloys.

1. Introduction

Tungsten heavy alloys (WHAs) have excellent properties such as high melting point, good thermal stability, high strength, and high radiation absorption capacity [1–3]. Therefore, WHAs are commonly used in many engineering applications including radiation shields, counterweight balance, electrical contacts, damping devices, and kinetic energy penetrators [4–7]. Nickel, iron, cobalt, and chromium are the most common elements added to a tungsten matrix and serve as a binder phase in tungsten heavy alloys. The presence of a binder phase can significantly improve the ductility of the materials [8]. Furthermore, the addition of Mo and Y_2O_3 in the WHAs can effectively reduce the grain size and increase the hardness and transverse rupture strength (TRS) [9–12]. Mo can also reduce the interface energy of WHAs and alters the liquid/solid phases during sintering [13]. In earlier studies, it demonstrates that the microstructure and sintering behavior of the W–Mo–Ni–Fe–Co heavy tungsten alloys were strongly influenced by the dispersed oxide particles [14].

The design of a new binder phase is an important issue in the development of the next generation of WHAs to achieve desired material performance. In recent years, high entropy alloys (HEAs) are attractive new materials, which define as a single solid-solution phase composed in an equimolar or near equimolar ratio with a small difference in atom radii (<15%) [15,16]. HEAs exhibit excellent characteristics such as high hardness, excellent ductility as well as promising resistance to wear, oxidation, and corrosion [16,17]. It has been reported that FeCoNiCrMn alloy system with a single-phase FCC structure exhibits high thermal stability and slow lattice diffusion in HEAs, which have great potential in high temperature material applications [18]. Nanoscale deformation twins frequently occur at the FeCoNiCrMn alloy system, which increases the strength, ductility, and toughness of materials [19]. In recent years, FeCoNiCrMn HEAs synthesized by a combination of mechanical alloying and spark plasma sintering (SPS) have attracted wide attention [20]. It has been proposed that ultrafine-grained HEAs with high compressive and tensile strengths (over 1900 and 1000 MPa) can be archived by the powder metallurgy route [21]. Pure tungsten-containing HEA phase was also fabricated by different sintering techniques [22].

Therefore, in this study, new model tungsten heavy alloys have been developed by the use of high entropy alloys as a binder phase with a secondary ball milling method. The four elements (Co, Ni, Fe, Cr) have been selected for a medium entropy alloy (MEA) as a binder phase added into the model WHAs. A two-stage ball milling has been introduced to synthesize the new model WHAs. The W–Mo matrix phase and the NiFeCoCr MEA binder phase were pre-milled separately. The two phases were then further milled by secondary ball milling for an additional milling time. This study aims to investigate the effects of the MEA binder phase, secondary ball milling, and different sintering temperatures on

* Corresponding author.No. 1, Sec. 2, Da Hsueh Rd., Shoufeng, Hualien, 97401, Taiwan.
  E-mail address: chunliang@gms.ndhu.edu.tw (C.-L. Chen).

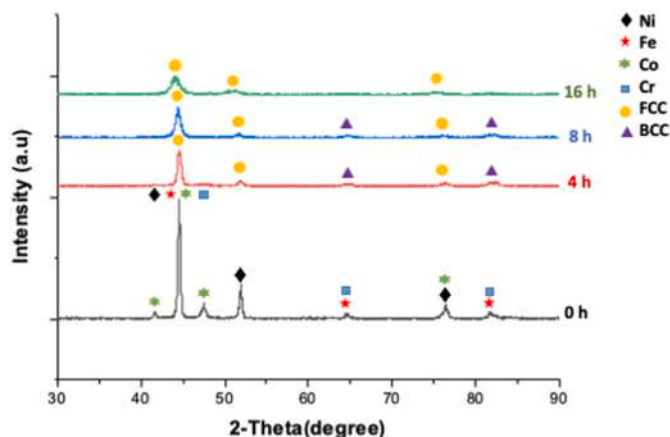| Model alloy		W	Mo	Ni	Fe	Co	Cr
W3Mo-10(FeCoNiCr)	(wt.%)	87	3	2.60	2.48	2.61	2.31
	(at.%)	69.4	4.6	6.5	6.5	6.5	6.5

Fig. 1. XRD spectra of the NiFeCoCr MEA powders milled for 0 h, 4 h, 8 h, and 16 h.

the characteristics, properties, and sintering behavior of the model WHAs. It is also important to understand the role of the MEA binder phase in the WHAs and how it interacts with the W–Mo matrix and influences the properties of the materials.

2. Materials and methods

The W–Mo model alloys reinforced with the NiFeCoCr binder phase fabricated by mechanical alloying were investigated. The raw materials used in this study were W, Mo, Ni, Fe, Co, and Cr elemental powders with a purity of 99.9% and particle size from 20 to 50 μm. A two-stage ball milling procedure was performed in this work. In the first stage of ball milling, the W–Mo matrix powders and NiFeCoCr MEA binder powders were pre-milled for 16 h, respectively. The matrix and binder phase powders were then further secondarily milled for 4 h, 8 h, 12 h, and 20 h. The chemical composition of the model alloy is given in Table 1 and named "W3Mo-10(NiFeCoCr)" in this study. Mechanical

alloying was carried out in a planetary ball mill (Retsch PM100) and operated at 300 rpm under an argon atmosphere for different milling times. Tungsten carbide was used as grinding media and the ball to powder weight ratio of 10:1 was selected for the ball milling procedure. The milled powders were consolidated by a green compact with a pressure of 210 MPa in 15 s and then sintered at three different temperatures (1250 °C, 1350 °C, and 1450 °C) for 60 min under a mixed hydrogen-argon atmosphere. Phase formation of the mechanically alloyed powders and sintered model alloys were analyzed by X'Pert PRO X-ray diffractometer (XRD). Microstructure evolution and chemical composition analysis were characterized by Hitachi-4700 scanning electron microscope (SEM) with energy-dispersive X-ray spectroscopy (EDS). Phase identification and crystal structure of the model alloys were further examined by a FEI Tecnai F20 G2 field emission gun transmission electron microscope (TEM). The Vickers hardness measurements were performed at room temperature by using a 1 kg load for 15 s. Nanoindentation measurements (MTS Nanoindenter XP) were used to obtain the hardness and elastic modulus using the continuous stiffness measurement (CSM).

3. Results and discussion

3.1. Characterization of the milled powders

3.1.1. XRD analysis of NiFeCoCr MEA binder powders

Fig. 1 shows the XRD spectra of the NiFeCoCr MEA binder powders as a function of milling time. The strongest diffraction peak of un-milled powders was observed at 2 theta of ~45°, corresponding to the overlapping of Ni, Fe, Co, and Cr elements. After 4 h of milling, the Co peaks at 2 theta of 42° and 47° were disappeared, suggesting that the alloying element was dissolved into the crystalline lattice through the formation of the solid solution during mechanical alloying. In the case of the early stage of milling, the unstable Ni-rich FCC and Cr-rich BCC phases were generated. With increasing milling duration up to 16 h, the XRD peaks shifting to the lower angle and broadening were apparently observed, indicating the formation of nanostructured powders and a complete FCC solid solution phase. It has been proposed that during a long milling duration the high stored energy can serve as a driving force to promote the formation of solid solution phases [23].

3.1.2. XRD analysis of heavy tungsten alloy powders

In this study, the W–Mo matrix phase and the NiFeCoCr MEA binder phase were pre-milled separately for 16 h. The two phases were then further milled by secondary ball milling for an additional milling time of
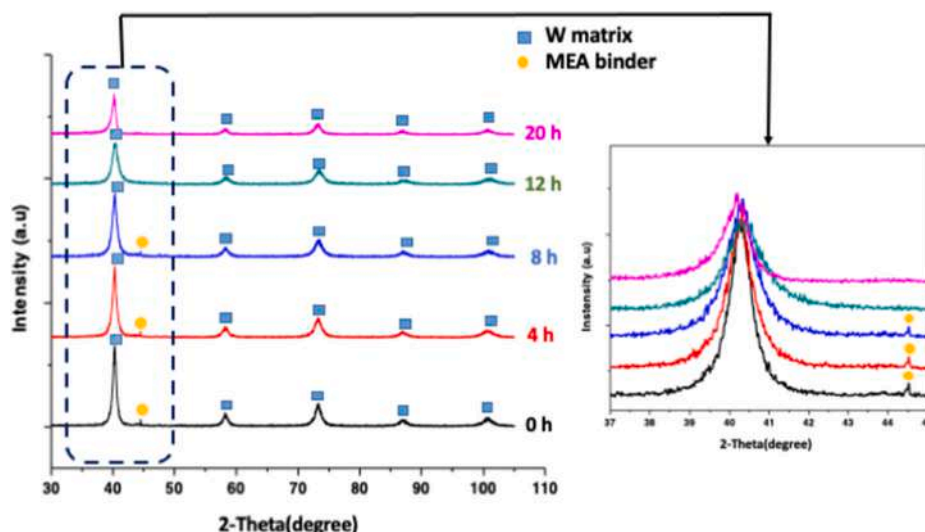
Fig. 2. XRD spectra of the W3Mo-10(NiFeCoCr) powders milled for 0 h, 4 h, 8 h, 12 h, and 20 h.
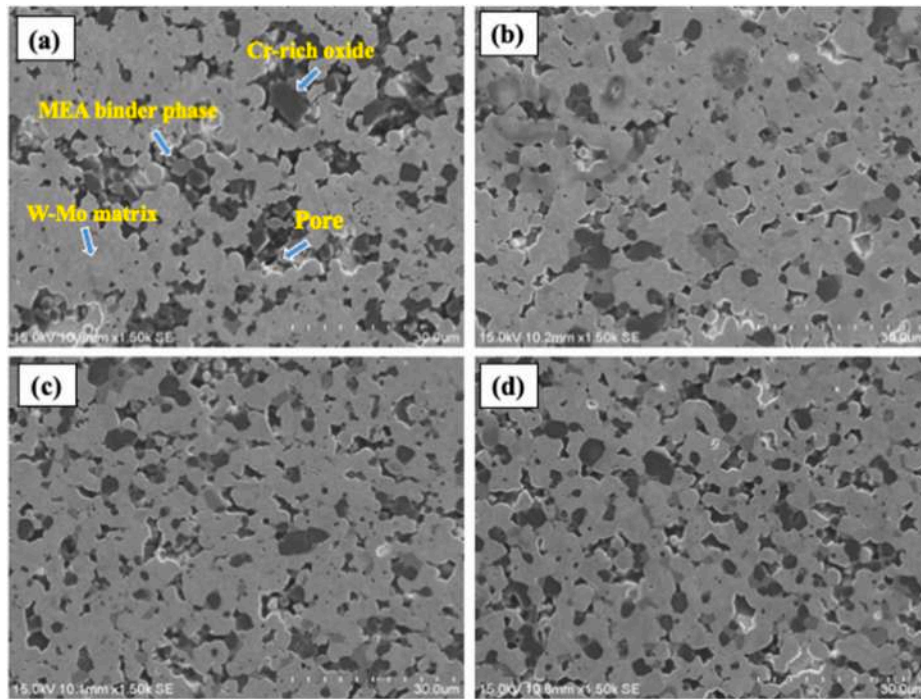
Fig. 3. SEM images of the W3Mo-10(NiFeCoCr) model alloys sintered at 1350 °C for the different milling times: (a) 4 h, (b) 8 h, (c) 12 h, and (d) 20 h.

4 h, 8 h, 12 h, and 20 h. Fig. 2 shows the XRD spectra of the W3Mo-10 (NiFeCoCr) powders milled as a function of milling time. In the starting powders (0 h), it can be seen clearly that the main peaks correspond to the W–Mo matrix phase and the weak peak at the low angle reflection (2 theta of ~45°) is associated with the MEA binder phase, see the enlarged image in Fig. 2. It should be noted that Mo was dissolved into W matrix to form the W–Mo solid solution phase from pre-alloyed powders of W–Mo. As a result, the Mo element was not detected in the 0 h of secondary ball milling. Additionally, the MEA binder phase with FCC structure was disappeared after the 12 h of secondary ball milling. It suggested that the diffusion of the MEA binder phase into the W–Mo crystalline lattice was generated. In this case, mechanical alloying plays an important role in promoting the formation of a solid solution during ball milling. As a consequence of an increase in milling durations, the intensity of W peaks can decrease gradually, which is related to that peak broadening and shifting. These effects can be associated with heavy deformation formed by mechanical alloying, resulting in a large number of crystal defects [24].

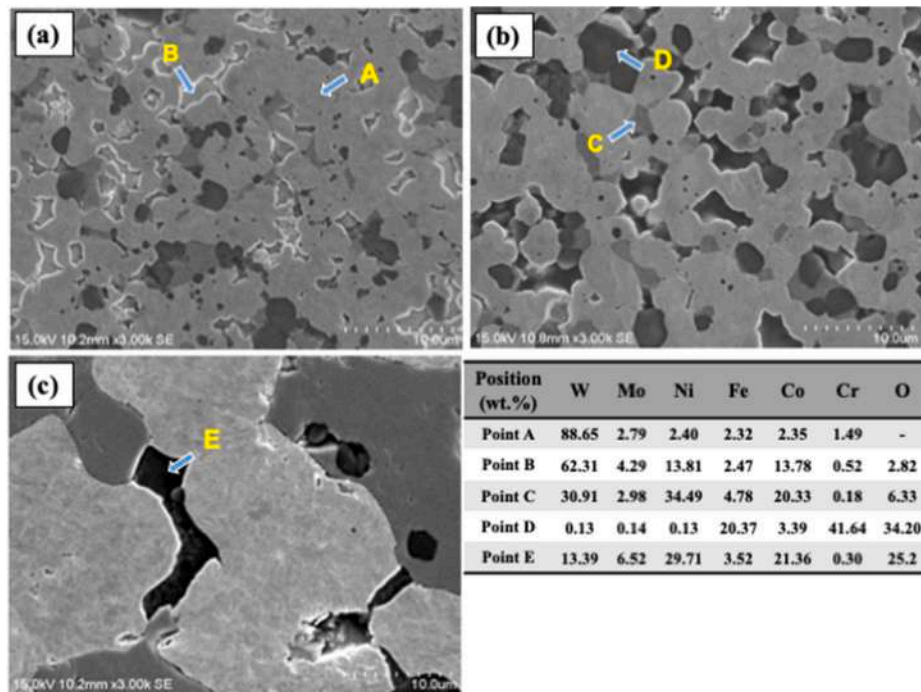| Position (wt.%)	W	Mo	Ni	Fe	Co	Cr	O
Point A	88.65	2.79	2.40	2.32	2.35	1.49	-
Point B	62.31	4.29	13.81	2.47	13.78	0.52	2.82
Point C	30.91	2.98	34.49	4.78	20.33	0.18	6.33
Point D	0.13	0.14	0.13	20.37	3.39	41.64	34.20
Point E	13.39	6.52	29.71	3.52	21.36	0.30	25.2

Fig. 4. SEM-EDS analysis of the W3Mo-10(NiFeCoCr) model alloys after milling for 20 h at different sintering temperatures: (a) 1250 °C, (b) 1350 °C, and (c) 1450 °C."
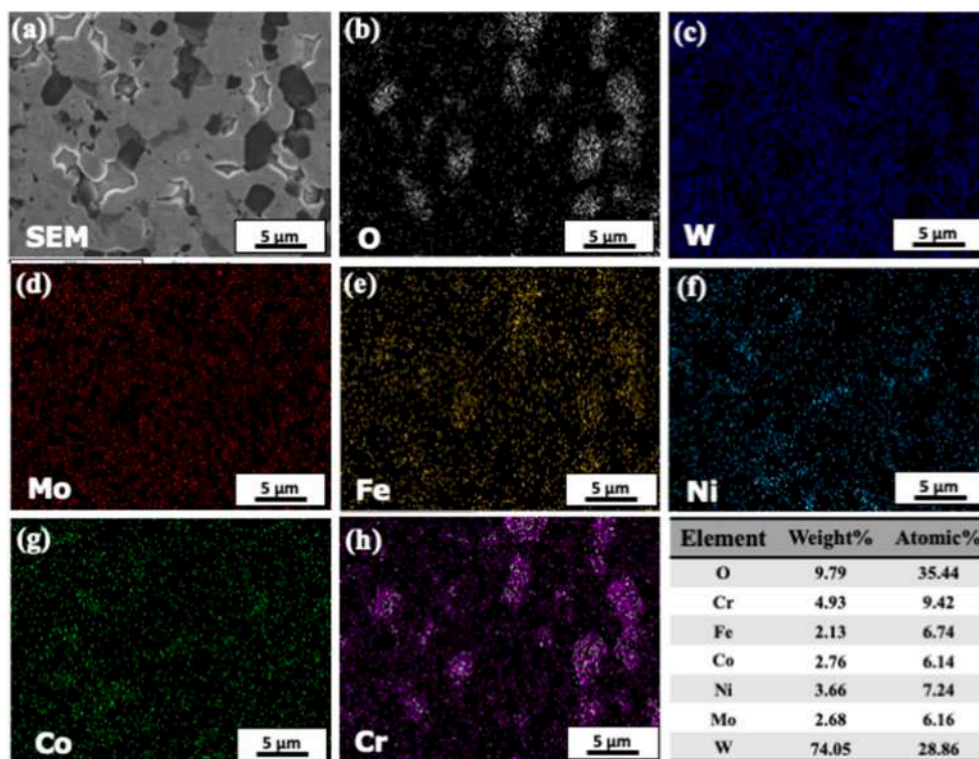
Element	Weight%	Atomic%
O	9.79	35.44
Cr	4.93	9.42
Fe	2.13	6.74
Co	2.76	6.14
Ni	3.66	7.24
Mo	2.68	6.16
W	74.05	28.86

Fig. 5. EDS mapping images of the W3Mo-10(NiFeCoCr) model alloy sintered at 1250 °C: (a) SEM image, (b) O map, (c) W map, (d) Mo map, (e) Fe map, (f) Ni map, (g) Co map, and (h) Cr map.

3.2. Characterization of the sintered model alloys

3.2.1. SEM observation and EDS analysis

Fig. 3 shows the microstructure evolution of the W3Mo-10 (NiFeCoCr) model alloys sintered at 1350 °C for the different milling times (4 h, 8 h, 12 h, and 20 h) by secondary ball milling. Fig. 3a illustrates that the model alloy milled for 4 h consists of the MEA binder phase (light gray), Cr-rich oxide (dark gray), and tungsten matrix with the inhomogeneous distribution of microstructure. Furthermore, segregation of the MEA binder phase and a number of small pores were also found in the microstructure, indicating an incomplete mechanical alloying process at the initial stage of milling. The microstructure of the model alloy is refined and tends to be uniform as the milling time increased to 8 h, see Fig. 3b. The MEA binder phase becomes more homogeneous and is distributed between the tungsten grains. After long milling durations, 12 h and 20 h, spherical-like binder phases in the range of 3~5 μm were observed and homogeneously distributed in the tungsten matrix as shown in Fig. 3c and d. It is evident that the morphology and distribution of the MEA binder phase and tungsten matrix can be considerably altered with increasing milling time. It has been reported that high-impact energy during the mechanical alloying process can promote grain refinement and nanostructured materials [24].

Fig. 4 Shows the SEM images and EDS analysis of the W3Mo-10 (NiFeCoCr) model alloys with the three different sintering temperatures. Fig. 4a exhibits the microstructure of the model alloy sintered at the low temperature of 1250 °C and it can be seen clearly that the small size of the MEA binder phase was obtained and homogeneously dispersed in the tungsten matrix. Point "A" indicates a bright region of the tungsten matrix, which contains a high level of tungsten and also small amounts of Mo, Ni, Fe, and Co elements. The result suggests that Mo can form a fully solid solution with tungsten during the pre-milling process. The subsequent secondary ball milling and sintering processes can lead to further interaction between the MEA binder phase and the W–Mo matrix phase. Furthermore, a large number of grains with a

bright edge are observed in the microstructure (see Point "B"), which has a high concentration of W with a low content of Ni, Co, and Fe elements. In this case, the low-temperature sintering of 1250 °C might cause insufficient migration of grain boundary and atom diffusion. Therefore, the brittle MEA binder phase could not have a good bonding strength with the W–Mo matrix. Consequently, it is most likely that the MEA binder phase fell out from the matrix during the sintering process.

Fig. 4b shows the microstructure of the model alloys after sintering at 1350 °C. The increase in the sintering temperature causes a significant grain growth of materials. The binder phase appeared as light gray, see Point "C", has a relatively high content of W, Ni, and Co elements. It should be noted that the W matrix can react with the MEA binder during ball milling and then a rapid diffusion occurred at high temperature sintering facilities high amounts of W dissolved in the MEA binder phase.

On the other hand, the high level of Cr, Fe, and O contents was found in the dark gray region as shown in Point "D", suggesting the formation of Cr-rich oxide. In this case, at high temperature sintering Cr can be redissolved from the MEA binder phase and promotes a great number of Cr-rich oxide formation. It has been reported that contamination (e.g., C, O, etc.) can be induced by the mechanical alloying process and the subsequent high temperature sintering promotes the formation of large size Cr-rich oxides due to Cr having a greater affinity for oxygen [25].

It is also confirmed that a considerable reduction of Cr content in the MEA binder phase, see Point "C", encourages the dissolution of Cr into the tungsten matrix to form the Cr-rich oxides as shown in Point "D". Therefore, it is evident to see that the Cr-rich oxide particles were frequently formed nearby the MEA binder phases.

As the sintering temperature was increased to 1450 °C, see Fig. 4c, it is apparently observed that the binder phase and tungsten grains grow rapidly up to ~20 μm. In this case, the liquid phase sintering was generated by the rapid diffusion of the MEA binder phase into the tungsten matrix where grains coarsen rapidly by coalescence. It is believed that once sufficient liquid forms spreading on the W–Mo powder particles the capillary force facilitates a rearrangement of
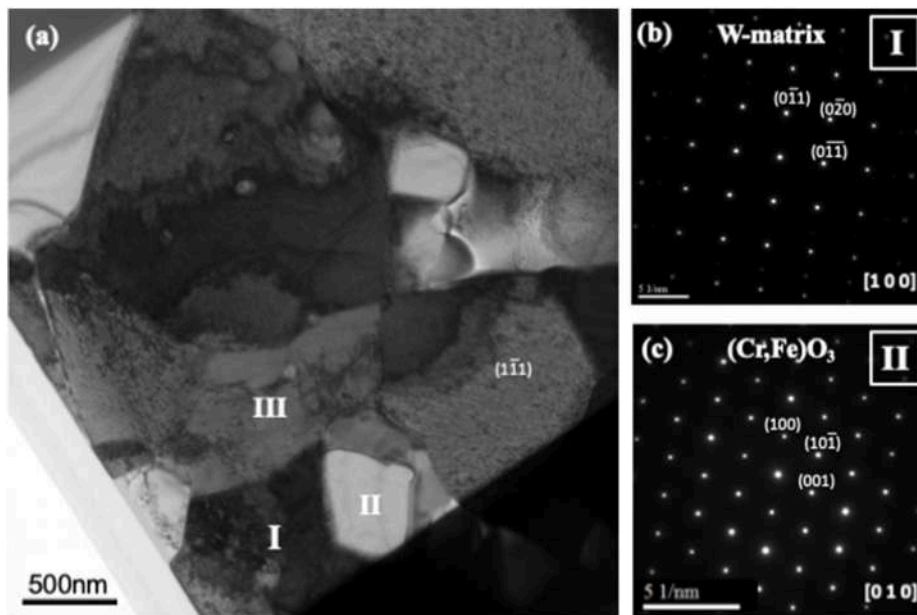
Fig. 6. TEM image of (a) the W3Mo-10(NiFeCoCr) model alloy sintered at 1250 °C and (b, c) the SAD patterns of the position "I" and "II" in Fig. 6(a).

powder particles and induces densification by liquid phase boning. It should be also noted that densification can also be determined by wettability during liquid state sintering, which can also be improved by increasing sintering temperature. Furthermore, the grain growth rate is sensitive to the sintering temperatures, which can be associated with solubility, diffusivity, surface energy, and volume fraction of the binder phase [26]. Fig. 4c also shows the dark region, see Point "E", where there is a very complicated oxide with the composition containing a high level of Ni, Co, W, and O elements. In this case, it is hard to identify the oxide

phase because the liquid phase can cause the rapid solution between the tungsten grain and the MEA binder phase. At the high sintering temperature of 1450 °C, it accelerates the instability and dissolution of the binder phase and thus tends to promote the complex oxide phase formation. It can be concluded that when the sintering temperatures were low (1250 °C or 1350 °C) the model alloys tend to behave as solid-phase sintering. However, as the sintering temperature was increased to 1450 °C, liquid phase sintering is dominant in the model alloys. The microstructure and densification of materials, as well as solubility of the
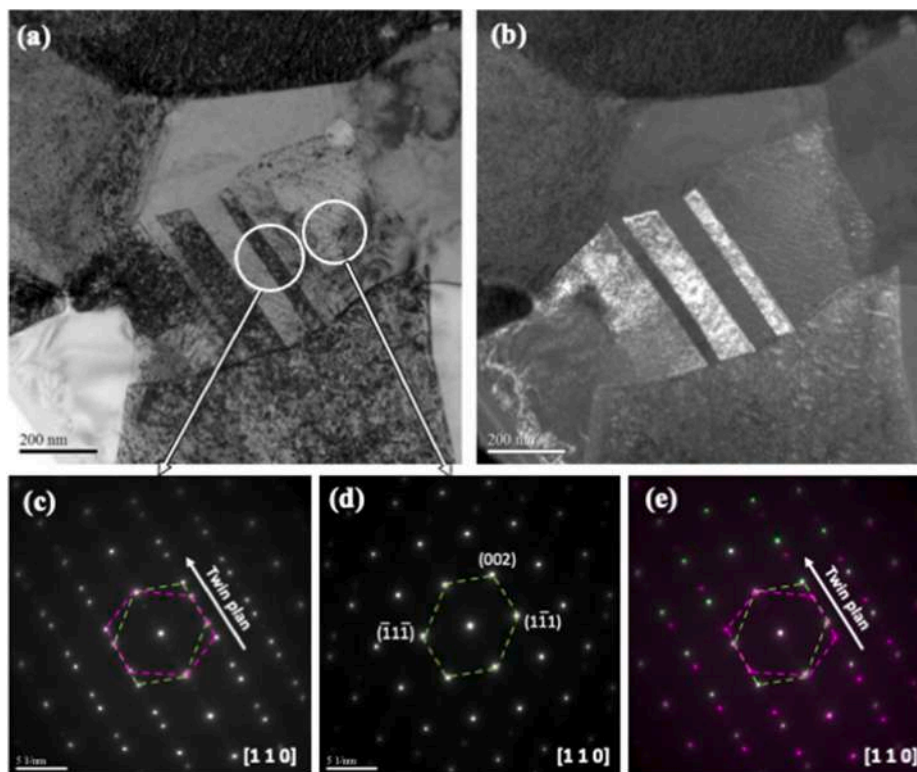

Fig. 7. TEM image of (a) bright field and (b) dark field of the MEA binder phase with twinned structure and (c–d) the SAD patterns of the twinned structure in Fig. 6(a).
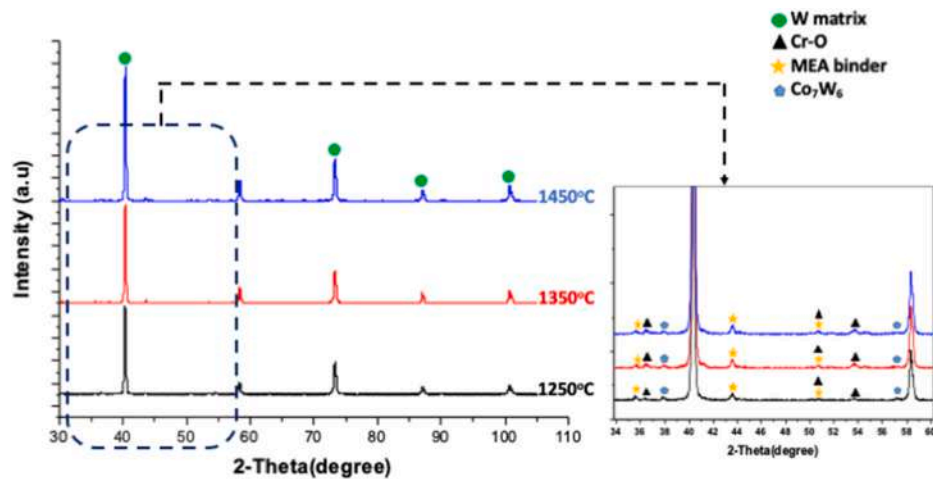
Fig. 8. XRD spectra of the W3Mo-10(NiFeCoCr) model alloys milled for 20 h at different sintering temperatures.

binding phase, can be altered as the sintering temperature increased from 1250 °C to 1450 °C.

Fig. 5 shows the EDS maps of the W3Mo-10(NiFeCoCr) model alloy sintered at 1250 °C. The W and Mo maps demonstrate the homogeneous distribution of elements in the microstructure, indicating a complete solid solution of the W–Mo matrix phase. However, the high concentration of the Cr, Fe, and O elements has been clearly observed in the EDS maps, which corresponds to Cr-rich oxides that appeared as a dark gray region in the SEM image as shown in Fig. 4. It has been proposed that the Cr and Fe elements have a lower Gibbs free energy than the Ni and Co elements and thereby facilitates oxidation reaction in the high entropy alloys [27]. Moreover, a high level of the Ni element, see the EDS map (Fig. 5f), suggests the formation of the MEA binder phase appeared as light gray in the SEM image, see Fig. 5a.

3.3. TEM observation

The W3Mo-10(NiFeCoCr) model alloy with the sintering temperature of 1250 °C was further examined by TEM. Fig. 6a shows that the microstructure of the model alloy sample has a grain size between 1 and 5 μm, which corresponds to solid-phase sintering, involving a small grain structure as shown in the SEM image of Fig. 4a. The dark region, see Point "I", contains a high W content with a small amount of Mo, indicating the tungsten matrix phase. The selected area diffraction (SAD) pattern of the tungsten matrix is oriented along the zone axis of [100] and has an average lattice parameter of 3.183 Å, see Fig. 6b. However, the bright area, see Point "II", has the composition of 61.2O–25.7Cr–10.7Fe-2.1Co (at.%), which can be related to the (Cr, Fe)-rich oxide. Phase identification was also performed using the SAD pattern as shown in Fig. 6c and the Cr–Fe–O oxide has been indexed as the (Cr, Fe)O$_3$ phase with an orthorhombic structure: a = 5.743 Å, b = 8.557 Å, c = 4.789 Å.

On the other hand, the MEA binder phase, see Point "III", appeared as light gray has a composition of 50.5Ni-23.31Co-6.81Fe-15.33 W (at %). It should be noted that the Cr free was found in the MEA binder phase, which suggests that the sintering process provides a rapid diffusion of Cr rejected from the supersaturated MEA binder phase. Thereby, the Cr-rich oxide is most frequently formed and observed in the model alloys.

The enlarged TEM micrographs of the MEA binder phase can be further seen in Fig. 7a (bright-field image) and Fig. 7b (dark-field image). According to SAD patterns, see Fig. 7c-e, the MEA binder phase has been identified as an FCC structure and is aligned along the [110] zone axis with an average lattice parameter of 3.685 Å. The twinned structure was clearly observed in the MEA binder phase. It has been proposed that the formation of the twinned binder phase could be
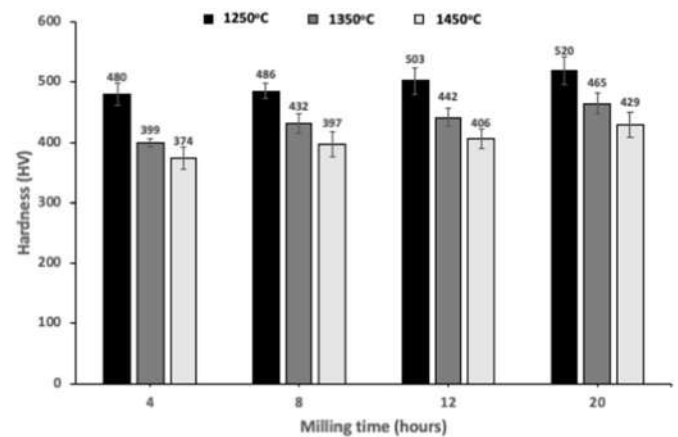

Fig. 9. The microhardness of the W3Mo-10(NiFeCoCr) model alloys at the different milling durations and sintering temperatures.

correlated with deformation-induced twinning during mechanical alloying [27]. In the case of the secondary ball milling, it provides a large strain deformation, which can promote the defect nucleation sites for deformation twins [26].

3.3.1. XRD analysis

Fig. 8 shows the XRD spectra of the W3Mo-10(NiFeCoCr) alloys for the different sintering temperatures. The strong diffraction peaks of W were clearly identified and the positions of the peaks are almost the same in the model alloys with the different sintering temperatures. However, the intensity of the W peaks tends to slightly increase as the sintering temperature increases due to grain growth or recovery occurred at the elevated temperatures. Additionally, in the enlarged XRD spectra, the small diffraction peaks were found and they correspond to the chromium oxides and MEA binder phase with FCC structure. It can be seen that the XRD results are in good agreement with the SEM observation as shown in Fig. 4.

3.4. Hardness and nanoindentation

Fig. 9 shows the microhardness of the W3Mo-10(NiFeCoCr) alloys for the different milling times and sintering temperatures. It is clear to observe that the increase of hardness is seen with increased time of milling. It is believed that the homogeneous microstructure with a fine grain size obtained after prolong milling was responsible for improving the hardness of alloys. However, with the increase of sintering
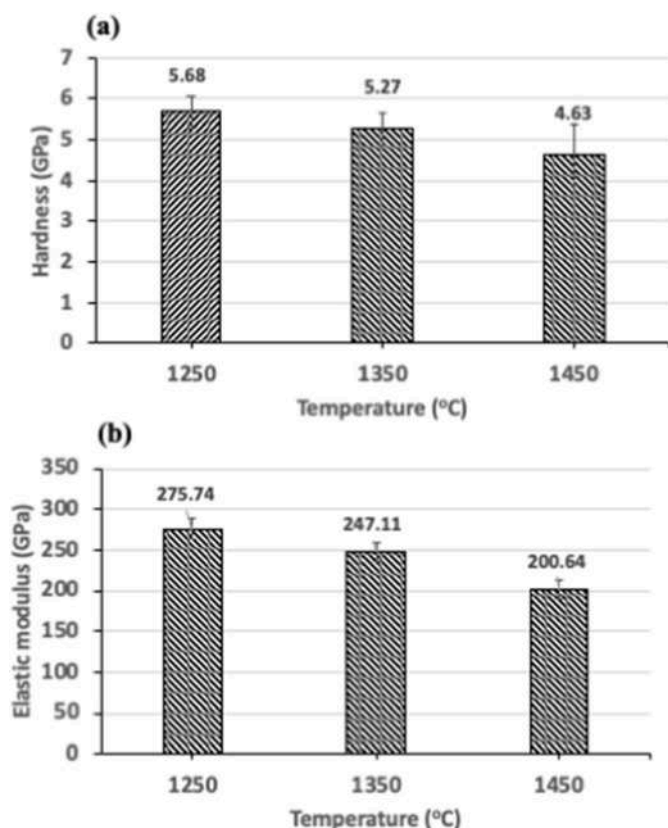
Fig. 10. Nanoindentation measurements of the W3Mo-10(NiFeCoCr) model alloys milled for 20 h at the different sintering temperatures: (a) hardness and (b) elastic modulus.

temperature, the hardness of the model alloys was decreased from 520 ± 23 HV (in average) at 1250 °C to 429 ± 20HV (in average) at 1450 °C. This suggests that a rapid diffusion rate occurred at high temperature facilities the formation of the liquid phase and significant growth in grain structure. Noted that a solid/liquid phase transition can be generated by increasing the sintering temperatures.

Fig. 10 shows the nanoindentation measurements of the W3Mo-10 (NiFeCoCr) model alloys at different sintering temperatures. It can be seen clearly that the hardness and elastic modulus of the model alloys increase with the decrease of the sintering temperatures. The results have a similar trend with Vickers hardness testing (see Fig. 9). It suggests

that the mechanical properties are strongly influenced by sintering temperatures, which dominate the grain structure, densification, solid/liquid phase transition, and homogeneity of the model alloys. Additionally, nanoindentation tests were performed on the individual phase of the model alloy sintered at 1450 °C, see Fig. 11. The results indicate that the tungsten matrix has a relatively higher hardness of 6.82 GPa and an elastic modulus of 258.2 GPa than the MEA binder phase with a hardness of 2.99 GPa and elastic modulus of 146.0 GPa as shown in Fig. 11. Therefore, the presence of the MEA binder and its grain size and distribution is essential in determining the mechanical properties of the model alloys.

4. Conclusion

The use of the equiatomic medium-entropy alloy (NiFeCoCr) as a binder phase in WHAs was synthesized by mechanical alloying. The effects of the MEA binder phase and sintering temperatures on microstructure characteristics and mechanical properties of the W3Mo-10 (NiFeCoCr) model alloys were studied. The pre-milling of the NiFeCoCr MEA binder phase shows that the formation of a single FCC solid-solution phase was obtained after 16 h of milling. SEM results illustrate that the morphology and distribution of the MEA binder phase and tungsten matrix can be considerably altered with increasing milling time. As the sintering temperature was increased to 1450 °C, liquid phase sintering is dominant in the model alloys. Furthermore, the Cr and Fe elements of the binder phase have a high affinity with oxygen and form Cr-rich oxides during the mechanical alloying and subsequent sintering process. It is evident to reveal that a considerable reduction of Cr content in the MEA binder phase encourages the dissolution of Cr into the tungsten matrix to promote the formation of Cr-rich oxides. TEM investigations also show that the Cr-rich oxide has been indexed as the $(Cr, Fe)O_3$ phase with an orthorhombic structure. The twinned structure was clearly observed in the MEA binder phase, which has been identified as an FCC structure. Regarding with mechanical properties, the hardness of the model alloys was decreased with the increase of sintering temperature. This suggests that a rapid diffusion rate occurred at high temperature facilities the formation of the liquid phase and significant growth in grain structure.

Author statement

Chun-Liang Chen: Methodology, Supervision, Writing- Original draft preparation, Conceptualization, Validation, Writing- Reviewing and Editing, Resources, Project administration. **Sutrisna:** Methodology, Software, Data curation, Visualization, Writing- Original draft
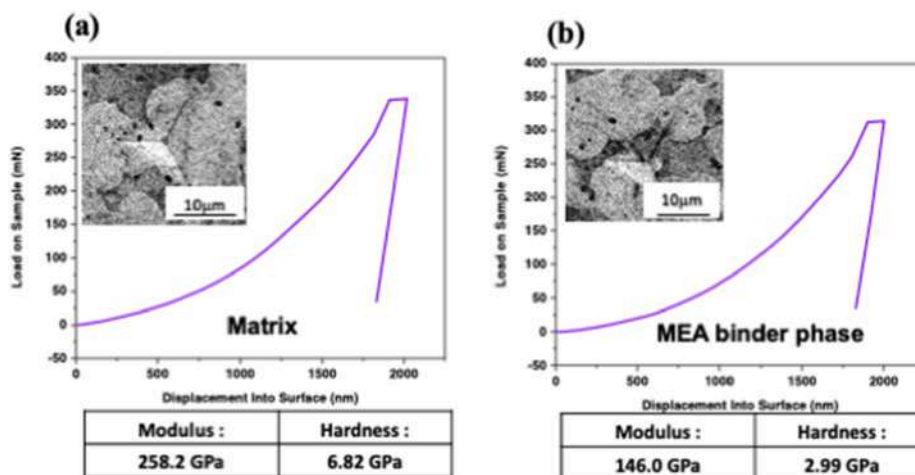

Fig. 11. Nanoindentation tests of the W3Mo-10(NiFeCoCr) sintered at 1450 °C: (a) tungsten matrix and (b) MEA binder phase.

preparation, Investigation.

Declaration of competing interest

The authors declare that they have no known competing financial interests or personal relationships that could have appeared to influence the work reported in this paper.

Acknowledgments

References

[1] Y. Şahin, Recent progress in processing of tungsten heavy alloys, J. Powder Technol. 2014 (2014), https://doi.org/10.1155/2014/764306.

[2] O. Dinçer, M.K. Pehlivanoḻlu, N.K. Çalişkan, I. Karakaya, A. Kalkanli, Processing and microstructural characterization of liquid phase sintered tungsten-nickel-cobalt heavy alloys, Int. J. Refract. Metals Hard Mater. 50 (2015) 106–112, https://doi.org/10.1016/j.ijrmhm.2014.12.009.

[3] K.H. Lee, S.I. Cha, H.J. Ryu, S.H. Hong, Effect of two-stage sintering process on microstructure and mechanical properties of ODS tungsten heavy alloy, Mater. Sci. Eng. 458 (2007) 323–329, https://doi.org/10.1016/j.msea.2007.01.118.

[4] A. Arora, V. Gopal Rao, Tungsten heavy alloy for defence applications, Mater. Technol. 19 (2004) 210–215, https://doi.org/10.1080/10667857.2004.11753087.

[5] A. Upadhyaya, S.K. Tiwari, P. Mishra, Microwave sintering of W-Ni-Fe alloy, Scripta Mater. 56 (2007) 5–8, https://doi.org/10.1016/j.scriptamat.2006.09.010.

[6] P. Lu, R.M. German, Multiple grain growth events in liquid phase sintering, J. Mater. Sci. 36 (2001) 3385–3394, https://doi.org/10.1023/A:1017943524875.

[7] R.M. German, K.S. Churn, Sintering atmosphere effects on the ductility of W-Ni-Fe, Heavy Metals 15 (1984) 94–95.

[8] C.L. Chen, S.H. Ma, Study on characteristics and sintering behavior of W-Ni-Co tungsten heavy alloy by a secondary ball milling method, J. Alloys Compd. 731 (2018) 78–83, https://doi.org/10.1016/j.jallcom.2017.09.125.

[9] N. Lin, C.H. Wu, Y.H. He, D.F. Zhang, Effect of Mo and Co additions on the microstructure and properties of WC-TiC-Ni cemented carbides, Int. J. Refract. Metals Hard Mater. 30 (2012) 107–113, https://doi.org/10.1016/j.ijrmhm.2011.07.011.

[10] G. Zhang, W. Xiong, Q. Yang, Z. Yao, S. Chen, X. Chen, Effect of Mo addition on microstructure and mechanical properties of (Ti,W)C solid solution based cermets, Int. J. Refract. Metals Hard Mater. 43 (2014) 77–82, https://doi.org/10.1016/j.ijrmhm.2013.11.004.

[11] Z. Zhao, J. Liu, H. Tang, X. Ma, W. Zhao, Effect of Mo addition on the microstructure and properties of WC e Ni e Fe hard alloys, J. Alloys Compd. 646 (2015) 155–160, https://doi.org/10.1016/j.jallcom.2015.05.277.

[12] C.L. Chen, C.L. Huang, Y. Zeng, Synthesis of ODS heavy tungsten alloys through post-annealing and secondary ball milling, Int. J. Refract. Metals Hard Mater. 48 (2017) 359–364, https://doi.org/10.1016/j.ijrmhm.2014.10.008.

[13] Z.A. Hamid, S.F. Moustafa, W.M. Daoush, F.A. Mouez, M. Hassan, Fabrication and characterization of tungsten heavy alloys using chemical reduction and mechanical alloying methods, Open J. Appl. Sci. 3 (2013) 15–27, https://doi.org/10.4236/ojapps.2013.31003.

[14] C.L. Che, Sutrisna, the effect of mo and dispersoids on microstructure, sintering behavior, and mechanical properties of W-Mo-Ni-Fe-Co heavy tungsten alloys, Metals 9 (2019) 1–11, https://doi.org/10.3390/met9020111.

[15] Y. Zhang, T.T. Zuo, Z. Tang, M.C. Gao, K.A. Dahmen, P.K. Liaw, Z.P. Lu, Microstructures and properties of high-entropy alloys, Prog. Mater. Sci. 61 (2014) 1–93, https://doi.org/10.1016/j.pmatsci.2013.10.001.

[16] J.W. Yeh, S.K. Chen, S.J. Lin, J.Y. Gan, T.S. Chin, T.T. Shun, C.H. Tsau, S.Y. Chang, Nanostructured high-entropy alloys with multiple principal elements: novel alloy design concepts and outcomes, Adv. Eng. Mater. 6 (2004) 299–303+274, https://doi.org/10.1002/adem.200300567.

[17] R. Rudolf, The Advantages of Modified Air Plasma Jet Method in the Process of Deposition of Hydroxyapatite Coatings on the Titanium Surface 56, 2015, pp. 3–8, https://doi.org/10.5937/ZasMat1502123J.

[18] B. Jia, X.J. Liu, H. Wang, Y. Wu, Z.P. Lu, Microstructure and mechanical properties of FeCoNiCr high-entropy alloy strengthened by nano-Y2O3 dispersion, Sci. China Technol. Sci. 61 (2018) 179–183, https://doi.org/10.1007/s11431-017-9115-5.

[19] F. Otto, A. Dlouhý, C. Somsen, H. Bei, G. Eggeler, E.P. George, The influences of temperature and microstructure on the tensile properties of a CoCrFeMnNi high-entropy alloy, Acta Mater. 61 (2013) 5743–5755, https://doi.org/10.1016/j.actamat.2013.06.018.

[20] W. Ji, W. Wang, H. Wang, J. Zhang, Y. Wang, F. Zhang, Z. Fu, Alloying behavior, and novel properties of CoCrFeNiMn high-entropy alloy fabricated by mechanical alloying and spark plasma sintering, Intermetallics 56 (2015) 24–27, https://doi.org/10.1016/j.intermet.2014.08.008.

[21] Y. Liu, J. Wang, Q. Fang, B. Liu, Y. Wu, S. Chen, Preparation of superfine-grained high entropy alloy by spark plasma sintering gas atomized powder, Intermetallics 68 (2016) 16–22, https://doi.org/10.1016/j.intermet.2015.08.012.

[22] P.V. Satyanarayana, R. Sokkalingam, P.K. Jena, K. Sivaprasad, K.G. Prashanth, Tungsten matrix composite reinforced with CoCrFeMnNi high-entropy alloy: impact of processing routes on microstructure and mechanical properties, Metals 9 (2019) 992, https://doi.org/10.3390/met9090992.

[23] J.Y. Huang, Y.D. Yu, Y.K. Wu, D.X. Li, H.Q. Ye, Microstructure and nanoscale composition analysis of the mechanical alloying of Fe x Cu 100-x (X= 16, 60), Acta Mater. 45 (1997) 113–124, https://doi.org/10.1016/S1359-6454(96)00163-2.

[24] C. Suryanarayana, E. Ivanov, V.V. Boldyrev, The science and technology of mechanical alloying, Mater. Sci. Eng. 304–306 (2001) 151–158, https://doi.org/10.1016/S0921-5093(00)01465-9.

[25] C.L. Chen, Suprianto, Effects of nano-dispersoids on synthesis and characterization of low Cr containing CoNiFeMnCr high entropy alloy by mechanical alloying, Intermetallics 113 (2019), 106570, https://doi.org/10.1016/j.intermet.2019.106570.

[26] C.L. Chen, S.H. Ma, Effects of Ni/Co ratio and mechanical alloying on characteristics and sintering behavior of W-Ni-Co tungsten heavy alloys, J. Alloys Compd. 711 (2017) 488–494, https://doi.org/10.1016/j.jallcom.2017.04.037.

[27] Y.J. Xu, K. Du, C.Y. Cui, H.Q. Ye, Deformation twinning with zero macroscopic strain in a coarse-grained Ni-Co-based superalloy, Scripta Mater. 77 (2014) 71–74, https://doi.org/10.1016/j.scriptamat.2014.01.030.